

Dimensional errors in LIGA-produced metal structures due to thermal expansion and swelling of PMMA

S K Griffiths, J A W Crowell, B L Kistler and A S Dryden

Sandia National Laboratories, Livermore, CA 94551-0969, USA

Received 23 April 2004

Published 9 August 2004

Online at stacks.iop.org/JMM/14/1548

doi:10.1088/0960-1317/14/11/017

Abstract

Numerical methods are used to examine dimensional errors in metal structures microfabricated by the LIGA process. These errors result from elastic displacements of the PMMA mould during electrodeposition and arise from thermal expansion of the PMMA when electroforming is performed at elevated temperatures and from PMMA swelling due to absorption of water from aqueous electrolytes. Both numerical solutions and simple analytical approximations describing PMMA displacements for idealized linear and axisymmetric geometries are presented and discussed. We find that such displacements result in tapered metal structures having sidewall slopes up to $14\ \mu\text{m}$ per millimetre of height for linear structures bounded by large areas of PMMA. Tapers for curved structures are of similar magnitude, but these structures are additionally skewed from the vertical. Potential remedies for reducing dimensional errors are also discussed. Here we find that auxiliary moat-like features patterned into the PMMA surrounding mould cavities can reduce taper by an order of magnitude or more. Such moats dramatically reduce tapers for all structures, but increase skew for curved structures when the radius of curvature is comparable to the structure height.

1. Introduction

The LIGA process [1–3] employs deep x-ray lithography and electrodeposition to produce metal structures having lateral dimensions up to several centimetres and feature sizes down to $1\ \mu\text{m}$ or somewhat less. Lithography for this process is performed using synchrotron radiation and a patterned absorber mask to expose a thick PMMA resist. The resist is developed to remove irradiated areas, producing a non-conducting PMMA mould, and the mould is then filled via electrodeposition to form either individual metal parts or a tool for making replicas by embossing or injection moulding.

Many factors influence the overall accuracy of a finished metal structure. Dimensional errors may result directly from errors in the PMMA mould due to synchrotron beam divergence [4, 5], fluorescence radiation [4–8], photoelectrons [4, 5, 9, 10] and thermal expansion of the mask [11]. These generally produce dimensional discrepancies between the

mask pattern and final structure of at most a few micrometres. Errors in metal structures can also result from elastic displacements of the PMMA during the electroforming process [12–14]. PMMA has a coefficient of thermal expansion of about $7 \times 10^{-5}\ \text{°C}^{-1}$ [15], so a rise in temperature of $30\ \text{°C}$ ($50\ \text{°C}$ plating temperature) gives a linear strain of more than 0.2%. Water absorbed from the electrolyte bath may produce even larger strains, up to 0.4% [12, 16], and the combined strains due to absorption and thermal expansion may reach 0.6%. Strains of this magnitude are fairly small, but they can nevertheless lead to large dimensional errors in LIGA-produced metal structures. As illustrated in figure 1, these errors are manifested mainly in the form of tapered metal structures having sidewall slopes up to about $14\ \mu\text{m}\ \text{mm}^{-1}$. Such errors exceed all lithographically-induced errors by an order of magnitude or more [1–11].

Only one previous study has addressed the impact of PMMA swelling on dimensional errors. Ruzzu and

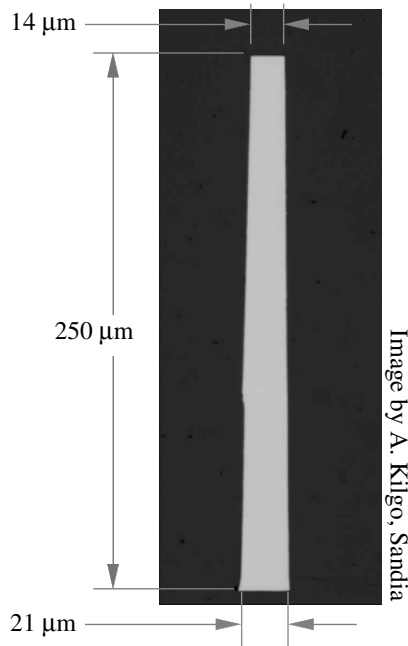


Figure 1. Optical micrograph in the cross-section of a LIGA-produced nickel structure electrodeposited at 50 °C. The width of this beam-like structure varies from 21 μm near the bottom to 14 μm at the top. Mean sidewall slopes are 14 μm mm⁻¹; overall taper is 28 μm mm⁻¹.

Matthis [12] examined both water absorption and thermal expansion of PMMA in nickel-sulfamate electrolyte and found that the combined strain reached about 0.5% at a temperature of 52 °C following 20 h of submersion. Their sample thickness was 1 mm. At 23 °C, they reported a total strain of about 0.1% following 100 h of submersion. They also investigated the effect of this strain on a specific annular feature. For a 500 μm resist thickness, they reported a growth of the radius of 7 μm at the top of the annulus at 52 °C, corresponding to a mean sidewall slope of 14 μm mm⁻¹; at 23 °C, this radial expansion was reduced by a factor of two. In this predominantly experimental effort, the authors additionally recommended improvements to the design that reduced dimensional errors and proposed an analytical expression for PMMA displacement along the sidewall of an annulus. This expression, based on an analogy to beam bending, was discussed only in the context of scaling and was not related to thermal or absorption strains.

The present paper addresses PMMA swelling and its effect on dimensional errors using theoretical means. To help understand and remedy these errors, we have computed sidewall displacements for PMMA features of various geometries and have fit the numerical solutions to obtain simple analytical expressions describing top-surface sidewall displacements as a function of the geometry and strain. Both linear and axisymmetric geometries are considered. The resulting expressions are useful in estimating dimensional errors for a variety of structure geometries and in the design of auxiliary features patterned into the resist to reduce these errors.

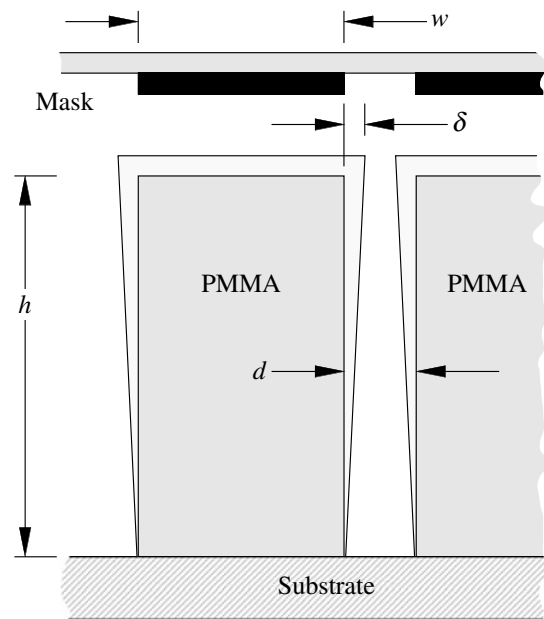


Figure 2. Schematic of sidewall displacements due to expansion of the PMMA. Sidewalls become sloped and slightly curved because the bottom surface is attached to a rigid substrate. Displacements δ scale with the height h when w/h is large.

2. PMMA strains and displacements

Goods *et al* [16] investigated PMMA swelling due to thermal expansion and water absorption for cases in which the PMMA is unconfined. They examined absorption-induced strains in de-ionized water and electrolyte baths of both nickel-sulfamate and nickel-Watts for three linear PMMA materials. They found that the rate of water absorption was strongly dependent on temperature, but that the equilibrium saturation and equilibrium swelling were remarkably insensitive to temperature between 4 and 50 °C. They further found that equilibrium strains do not vary much with material type, but do depend on bath composition. The reported equilibrium linear strain for water was about 0.41%, that for nickel-Watts was 0.38% and that for nickel-sulfamate was about 0.28%. Their reported value for the linear coefficient of thermal expansion was $\sim 7.5 \times 10^{-5} \text{ } ^\circ\text{C}^{-1}$ for all three PMMA materials.

Now consider the geometry shown in figure 2 depicting a mask, developed PMMA and a substrate typical of LIGA. The mask here defines a long linear feature in the PMMA having a nominal width w and height h , and this PMMA bounds a linear mould cavity of nominal width d . If this PMMA were a part of a simply connected freestanding sheet, and if strains in the PMMA were uniform and isotropic, then all of these dimensions, including the cavity width, would simply grow by the magnitude of the linear strain when the PMMA expands. In such a case, the PMMA sidewalls would remain parallel and vertical, and relative dimensional errors in the metal structure would be identical to the total strain. This is at most about $\varepsilon = 0.6\%$ accounting for both thermal expansion and absorption of water, so the absolute error in a metal structure 100 μm wide would be only about 0.6 μm. Such errors would be quite acceptable for nearly all applications of LIGA.

Moreover, even these small errors could be corrected with ease using an appropriately scaled mask pattern.

Uniform and isotropic expansion of the PMMA is not possible, however, because the resist is bonded to a rigid substrate. The role of this substrate is to hold isolated PMMA features in their correct relative positions and to provide a continuous conductor for electrodeposition. The substrate and adhesion to the substrate are thus essential elements of the process. Further, the coefficient of expansion of all common substrate materials is negligible in comparison to that of PMMA, and these materials do not absorb water. Confinement by the substrate consequently requires nearly zero displacement of the PMMA at the substrate interface. Under this condition, PMMA expansion yields sidewall displacements into the mould cavity in regions above the substrate, producing a tapered metal structure and potentially large dimensional errors.

When the PMMA is confined by a substrate and the width w of the PMMA is large, each top-surface sidewall displacement δ is about twice the product of the strain and the resist thickness (this is demonstrated shortly). In this case, the error in the width of a metal structure is $2\delta \approx 4.6\epsilon h$, and this yields a top-surface error of about $28 \mu\text{m}$ for a total strain of 0.6% and a structure height $h = 1 \text{ mm}$. Here the structure discussed above will have the nominal width of $100 \mu\text{m}$ at the bottom, but the top-surface width will be only $72 \mu\text{m}$. Such dimensional errors are unacceptable in metal piece-parts for all but rudimentary applications, and tapered structures cannot be corrected using a scaled or biased mask pattern. Moreover, replication tools fabricated by over-plating the resist may exhibit large adverse sidewall drafts, leading to tool damage or damage to the replica during moulding or embossing.

3. Linear features

We first examine long linear features as shown previously in figure 2. Without loss of generality, the width and displacements can be considered in the dimensionless form w/h and $\delta/\epsilon h$. For this geometry, normalized top-surface lateral displacements were computed using ABAQUS [17] over a wide range of the normalized width. Swelling was represented by a uniform isotropic unit strain, and because sidewall displacements are always proportional to the strain when strains are small, the normalized displacement depends only on w/h . Boundary conditions used for these calculations are zero displacement on the lower surface; all other boundaries are free surfaces. Poisson's ratio for PMMA is taken as $\nu = 0.35$ [17], and the plane-strain approximation is employed as appropriate for long features.

The numerical solutions are shown in figure 3 (symbols) in the form of the normalized displacement $\delta/\epsilon h$ as a function of the normalized width w/h . These values were fit to obtain a simple analytical expression describing the normalized top-surface sidewall displacement as a function of the geometry and strain. The result is

$$\frac{\delta}{\epsilon h} = f(\omega) = \frac{162\omega + 49\omega^3}{240 + 43\omega + 21\omega^3} \quad \omega = \frac{w}{h} \quad (1)$$

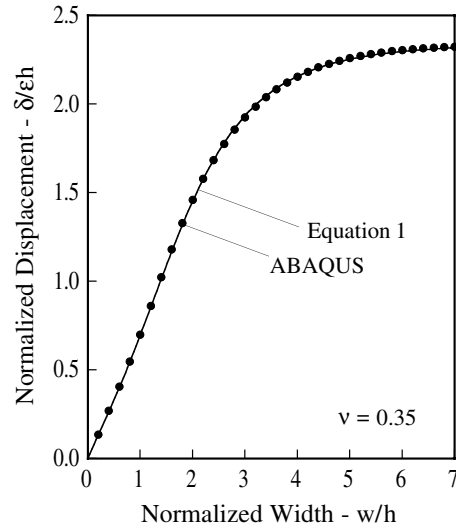


Figure 3. Normalized displacement of top-surface sidewall for long linear features. Displacements grow with increasing width w of the PMMA feature until the width is about five times the PMMA thickness h .

where again ϵ is the total linear strain, h is the PMMA thickness and w is the PMMA feature width. A plot of this function is also shown in figure 3 (curve). The relative discrepancy between this analytical result and the numerical solutions is less than 3% over the full range of widths. Note that the displacements of equation (1) are proportional to the sum $1 + \nu$ for the plane-strain conditions of long linear features, so the results of this expression can be scaled accordingly for values of Poisson's ratio other than 0.35. Also note that the correct asymptotic behaviour for top-surface displacement as defined in figure 2 is $\delta = \epsilon w(1 + \nu)/2$ when w/h is small; the value $162/240 = 0.675$ is identical to $(1 + \nu)/2$ for $\nu = 0.35$.

We see in figure 3 that normalized displacements depend strongly on the feature width when w/h is small, but are independent of the width when w/h is large. This is also apparent from the asymptotic behaviour of equation (1). For small and large widths, the asymptotes are

$$\delta \approx 0.68\epsilon w \quad \text{as} \quad \frac{w}{h} \rightarrow 0 \quad (2a)$$

and

$$\delta \approx 2.3\epsilon h \quad \text{as} \quad \frac{w}{h} \rightarrow \infty. \quad (2b)$$

Accordingly, lateral displacements are proportional to the PMMA feature width and independent of h when w/h is small; however, they are independent of w and proportional to the PMMA thickness when w/h is large.

The form of equation (2b) indicates a particularly serious problem of dimensional errors in metal structures. Given a cavity width d and symmetric PMMA features defining this cavity, the relative error e/d in the structure width can be expressed as

$$\frac{e}{d} = \frac{2\delta}{d} \approx 4.6\epsilon \frac{h}{d} = 4.6\epsilon A \quad \frac{w}{h} > 5 \quad (3)$$

where $A = h/d$ is the aspect ratio of the metal structure. For a linear structure, the relative error in the structure width is

thus proportional to the structure aspect ratio when the lateral extent of the PMMA bounding the structure is large compared to the height. Moreover, the magnitude of this error is large even for modest aspect ratios. For an aspect ratio of just 10 and a total strain of 0.006, the expected relative error is 28% for $w/h > 5$; it is still nearly 10% at this aspect ratio for a total strain of just 0.2%. Ruzzu and Matthis [12] noted that errors in their metal structures were about half of those measured in the PMMA, but this cannot be expected to be true for all PMMA geometries.

Equation (3) also indicates that PMMA displacements will limit the maximum producible aspect ratio of a metal structure when w/h is large. If the combined displacement $e = 2\delta$ exceeds the cavity width d , then the cavity will close at the top. The condition $e/d = 1$ therefore defines the maximum aspect ratio as $h/d = 1/4.6\epsilon$, and the value of this maximum is just 36 for a strain of 0.6%. The maximum aspect ratio increases to 72 for a strain of 0.3%.

To further illustrate the use of these equations, consider a resist of height $h = 100 \mu\text{m}$, a PMMA feature width of $w = 1000 \mu\text{m}$ and a total linear strain of 0.006. These dimensions yield $\omega = w/h = 10$, and equation (1) for this value gives $\delta/\epsilon h = 2.3$ or $\delta = 1.4 \mu\text{m}$ for each sidewall displacement. Increasing the height to $250 \mu\text{m}$, but leaving all else the same, the normalized width becomes $\omega = 4$, and equation (1) gives $\delta/\epsilon h = 2.15$ or $\delta = 3.2 \mu\text{m}$. Here the height increased by a factor of 2.5, and the displacement increased by 2.3. This is an expression of the linear scaling of equation (2b) for cases in which w/h is large. Increasing the height again to $1000 \mu\text{m}$ yields $\omega = 1$ and $\delta/\epsilon h = 0.69$ or $\delta = 4.2 \mu\text{m}$. Now, a factor of four increase in the height increased the displacement by only 40%, and this is an expression of the transition to equation (2a). Indeed as the height increases still further, the displacement becomes independent of height and is instead determined entirely by the PMMA feature width, which is fixed in the present example. In this limit, the displacement is always $4.0 \mu\text{m}$. Note that this is slightly smaller than the displacement for $h = 1000 \mu\text{m}$, so displacements do not always increase monotonically with increasing height. For $w = 1000 \mu\text{m}$, the maximum displacement is $\delta \approx 4.4 \mu\text{m}$, and this occurs for $h \approx 575 \mu\text{m}$.

Now consider a geometry in which the height is fixed but the cavity is bounded by PMMA features of variable width. Equation (1) again yields the limit $\delta = 2.3\epsilon h$ for large w/h . However, displacements are reduced from this limit by a factor of 3.3 to $\delta = 0.69\epsilon h$ for $w/h = 1$. For $w/h = 0.5$, the displacement is reduced by 7, and for $w/h = 0.2$ the reduction is a factor of almost 18. Dimensional errors due to PMMA swelling and thermal expansion can thus be reduced by more than an order of magnitude through controlling the geometry of the PMMA near mould cavities. This is discussed further in a later section on potential remedies.

In addition to sidewall displacements, strains due to thermal expansion and water absorption may lead to buckling of PMMA features when their aspect ratio is large. To examine this issue, the ABAQUS code was used to compute minimum strains for the onset of buckling of long linear PMMA features. This bifurcation buckling analysis yields the least-stable mode of deformation and the accompanying minimum strain as a function of the normalized width w/h and the ratio L/h

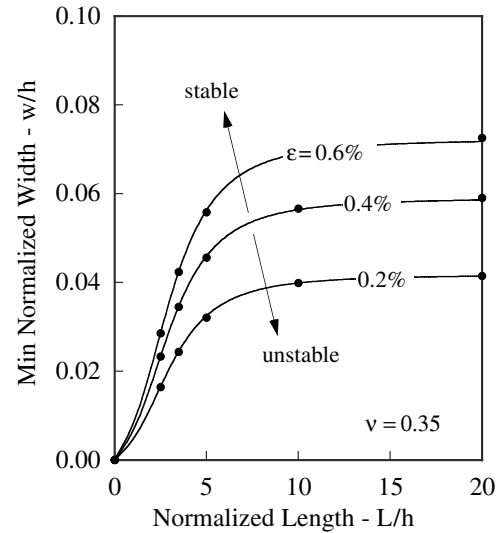


Figure 4. Minimum normalized feature width for stable PMMA features. Features of widths smaller than these values will buckle, producing wavy sidewalls at the top of a metal structure.

where L is the feature length. As before, these features are constrained to zero displacement on the lower boundary; all other surfaces are free boundaries, including the feature ends. In all cases examined, the least-stable mode was a periodic deformation of the top surface having a wavelength about five times the height provided the length-to-height ratio was large. The magnitudes of the buckling displacements were not computed; however, any such buckling is likely to result in unacceptable dimensional errors.

The computational results are shown in figure 4 (symbols) as the critical normalized width w/h in terms of L/h for various values of the strain. This is the minimum value of w/h for which buckling will not occur for a prescribed normalized length and strain. Regions above or to the left of each curve are therefore stable; those below or to the right will buckle. These numerical results are well approximated by

$$\frac{w_{\min}}{h} = \sqrt{\epsilon} \frac{46\lambda + 14\lambda^3}{497 + 72\lambda + 15\lambda^3} \quad \lambda = \frac{L}{h}. \quad (4)$$

This result is also shown in figure 4 (curves). The asymptotic behaviour of this expression for large L/h is $w_{\min}/h \approx 0.93\sqrt{\epsilon}$. As such, the maximum stable aspect ratio h/w for a very long PMMA feature ($L/h > 10$) is inversely proportional to the square-root of the strain. For a strain of 0.6%, this maximum aspect ratio is about 14. Shorter features ($L/h < 5$) are stable at much higher aspect ratios.

4. Axisymmetric features

We now examine sidewall displacements for axisymmetric features in the patterned PMMA. A schematic of such a feature and the associated nomenclature are shown in figure 5. Here the geometry is specified by the height h , and inner and outer radii r_i and r_o , or one radius and a width w . The behaviour of these annular features is much more complex than that of linear features, so several special cases will be investigated.

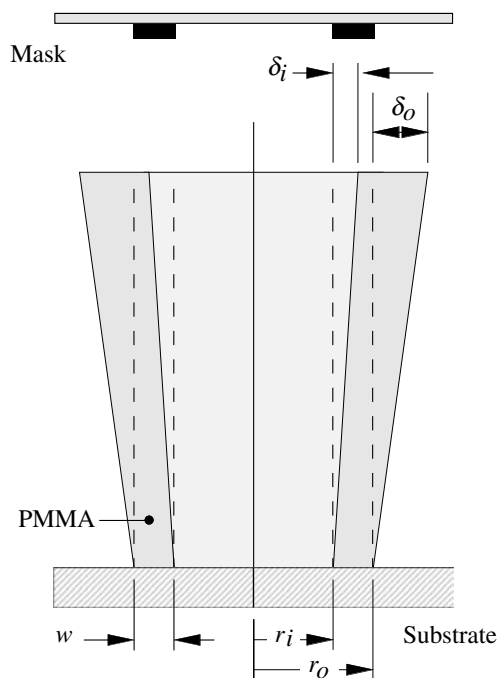


Figure 5. Schematic of axisymmetric feature. Thermal expansion and water absorption result in a PMMA feature that is wider at the top and skewed outward from the initial vertical position.

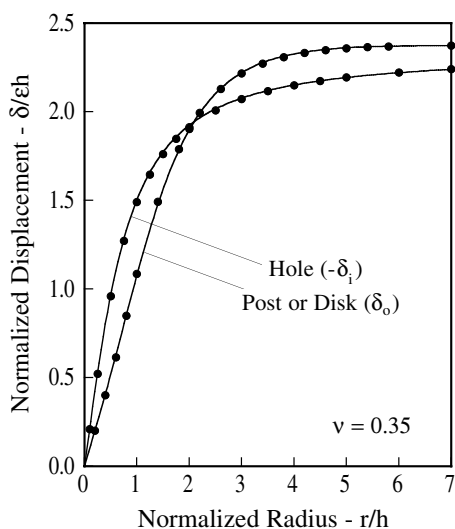


Figure 6. Normalized top-surface sidewall displacements for an isolated hole in PMMA and a PMMA post or disc. Maximum sidewall displacements always occur at the top surface.

The two simplest cases of axisymmetric geometry are the isolated hole and the post (or disc). The first of these corresponds to a prescribed inner radius and the limiting condition $r_o \rightarrow \infty$; as a practical matter this condition can be considered as $w/h > 7$. Figure 6 shows the computed normalized top-surface displacement (symbols) on the inner radius of such a hole as a function of the normalized inner radius $\rho_i = r_i/h$. As with the linear features discussed above, boundary conditions used in these calculations are zero displacement on the lower surface and stress-free surfaces everywhere else. These numerical results were fit to obtain

$$\frac{\delta_i}{\epsilon h} = -g(\rho_i) = -\frac{26\rho_i + 49\rho_i^2}{13 + 16\rho_i + 21\rho_i^2} \quad \rho_i = \frac{r_i}{h}. \quad (5)$$

This expression is shown in figure 6 by the curve labelled ‘hole’. The maximum discrepancy between equation (5) and the numerical results is about 4% for all radii and thicknesses. Note that the correct asymptotic behaviour for top-surface radial displacement of a hole boundary is $\delta_i = -\epsilon r_i(1 + \nu)/(1 - \nu)$ when r_i/h is small. The value $26/13 = 2$ in equation (5) thus approximates the ratio $(1 + \nu)/(1 - \nu) \approx 2.08$ for $\nu = 0.35$.

From equation (5), it is straightforward to show that the relative error in the diameter $2r$ of a metal post or disc produced in a cylindrical mould cavity is

$$\frac{e}{2r} = \frac{2\delta_i}{2r} \approx 2.3\epsilon \frac{h}{r} = 4.6\epsilon A \quad A = \frac{h}{2r} < 0.05 \quad (6a)$$

$$\frac{e}{2r} = \frac{2\delta_i}{2r} \approx 2\epsilon \quad A = \frac{h}{2r} > 1. \quad (6b)$$

This behaviour qualitatively differs from that of a linear feature as given in equation (3). Here the relative error scales with the aspect ratio only when the aspect ratio is small. For high aspect ratios, the relative error is independent of both the radius and height. As such, PMMA displacements never limit maximum aspect ratios for metal posts.

Figure 6 additionally shows computed normalized displacements for a PMMA post or disc as a function of the normalized outer radius $\rho_o = r_o/h$. Here the width w and outer radius r_o are equal, and the inner radius is zero. These numerical results are well described by

$$\frac{\delta_o}{\epsilon h} = q(\rho_o) = \frac{96\rho_o + 49\rho_o^{8/3}}{96 + 18\rho_o + 21\rho_o^{8/3}} \quad \rho_o = \frac{r_o}{h} \quad (7)$$

and the accuracy of this expression is better than 2%. In this case, relative errors in the diameter of a hole in a metal structure produced from a PMMA post are

$$\frac{e}{2r} = \frac{2\delta}{2r} \approx 2.3\epsilon \frac{h}{r} = 4.6\epsilon A \quad A = \frac{h}{2r} < 0.1 \quad (8a)$$

$$\frac{e}{2r} = \frac{2\delta}{2r} \approx \epsilon \quad A = \frac{h}{2r} > \frac{1}{2}. \quad (8b)$$

Relative errors for metal posts and holes in metal thus exhibit similar behaviour.

Displacements for both holes and posts in PMMA are defined such that a positive displacement increases the radius; negative displacements reduce the radius. Consequently, metal posts or discs (formed in PMMA holes) will always have a reduced radius at the top; the top surfaces of holes (formed around PMMA posts) will always be enlarged. Moreover, these results describe the maximum sidewall deviation of a metal structure as the maximum sidewall deviation of these PMMA features always occurs at the top surface.

PMMA displacements in axisymmetric geometries are more complex for features having an inner radius that is nonzero and an outer radius that is finite. For such annular features, displacements of the inner and outer radii differ significantly, and normalized forms of these displacements no longer exhibit simple monotonic growth with increasing feature width.

Top-surface displacements on the inner radius of annular PMMA features were computed using ABAQUS for

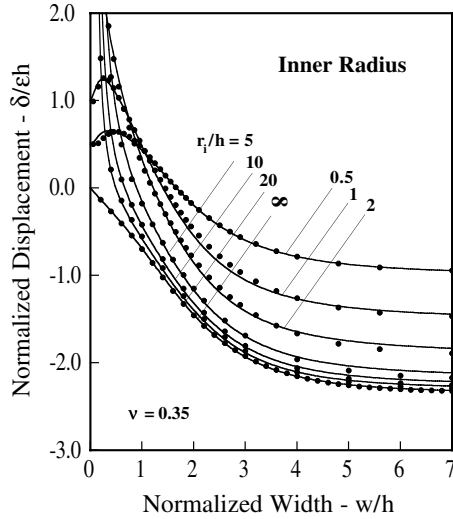


Figure 7. Normalized top-surface displacements on the inner radius of an axisymmetric PMMA feature. Inner-radius displacements may be positive or negative and pass through zero.

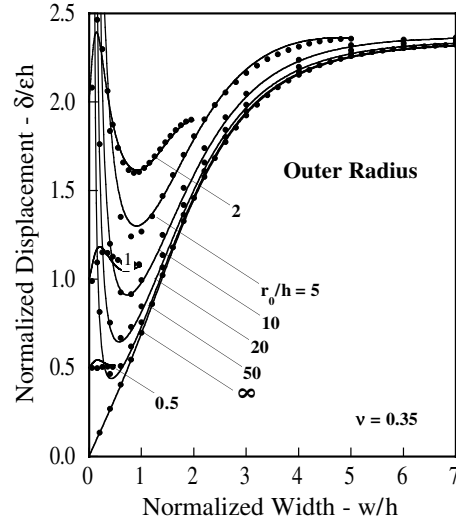


Figure 8. Top-surface displacements at the outer radius of an axisymmetric PMMA feature. Displacements are always positive, but exhibit minima at some optimum value of w/h .

prescribed values of the normalized inner radius $\rho_i = r_i/h$ and normalized width $\omega = w/h$. The numerical results (symbols) are shown in figure 7. Here we see that top-surface displacements are positive and proportional to the radius in the limit $w/h \rightarrow 0$. For any fixed and finite radius, these displacements increase with increasing width when the width is small, but reach a maximum and then decrease for still larger w/h . The displacements cross zero and become negative for sufficiently large w/h , approaching asymptotic values that depend only on the radius. These asymptotes are the displacements for holes given previously in figure 6 and equation (5).

Based on these observations, we find that the numerical solutions of figure 7 can be approximated by a composite expression using the displacements for linear features and holes. The result is

$$\frac{\delta_i}{\varepsilon h} = -(1 - \beta^2)f(\omega) - \beta^2g(\beta^2\rho_i) + s(\bar{\rho}, \omega) \quad (9a)$$

$$\beta = \frac{w}{r_o} = \frac{\omega}{\rho_o} = \frac{\omega}{\rho_i + \omega} \quad \bar{\rho} = \frac{\rho_i + \rho_o}{2} \quad (9b)$$

where the function f is given by equation (1) and the function g is given by equation (5). Here the argument of the function g is $\beta^2\rho_i$. Results from this expression are also shown in figure 7 (curves); these agree with the numerical results to within an absolute error of 0.12 for all values of the radius and feature width.

The first two terms of equation (9a) represent a weighted average of the displacements for a linear feature (dominant for $\beta \ll 1$) and those for a hole (dominant for $\beta \rightarrow 1$). The remaining term accounts for skewing of the feature, which is dominant when $\bar{\rho}$ is large but the product $\bar{\rho}\omega$ is small. It is given by

$$s(\bar{\rho}, \omega) = \bar{\rho} \left[\frac{9 + 8\bar{\rho}\omega + 320\omega^2}{9 + 227\omega^2 + 87\bar{\rho}^2\omega^3 + 6\bar{\rho}^3\omega^3} \right]. \quad (10)$$

The asymptotic behaviour of this expression is

$$s \approx \bar{\rho} \quad \text{as } \bar{\rho}\omega \rightarrow 0 \quad (11a)$$

$$s \approx \frac{4\bar{\rho}}{3(\bar{\rho}\omega)^2} \approx 0 \quad \text{as } \bar{\rho}\omega \rightarrow \infty. \quad (11b)$$

Skewing is therefore most significant when the radius r_i is large and the width w is very small such that $wr_i \ll h^2$.

Note that the term $s(\bar{\rho}, \omega)$ is the only positive contribution to the displacements of equation (9a) and that the zero crossing arises from a balance between outward (positive) skewing and inward (negative) displacements due to expansion of the feature wall. The condition yielding this zero of the net displacement is roughly

$$\omega_z \approx \frac{27\rho_i^{1/3} + 16\rho_i^2 + 13\rho_i^3}{10\rho_i(3 + \rho_i^{7/3})}. \quad (12)$$

Equation (12) therefore provides something of an optimum condition, but only in the sense that the top- and bottom-surface displacements are both zero. Displacements at intermediate positions along the feature height are not zero, but are nevertheless relatively small.

Similar results for displacements on the outer radius are shown in figure 8. Symbols represent results computed using ABAQUS, and positive displacements correspond to an increased radius. As with inner-radius displacements, top-surface outer-radius displacements are positive and proportional to the radius in the limit $w/h \rightarrow 0$. However, displacements of the outer radius are always positive, and these displacements exhibit a minimum instead of a zero crossing. This is because the individual contributions from skewing and expansion of the feature wall are both positive on the outer radius.

The numerical solutions in figure 8 were also fit by way of a composite expression, this time using the displacements for linear features and posts as the basis functions. Here the result is

$$\frac{\delta_o}{\varepsilon h} = (1 - \beta^3)f(\omega) + \beta^3q(\rho_o) + (1 - \beta^{5/3})s(\bar{\rho}, \omega) \quad (13)$$

where the function f is given by equation (1), q is given by equation (7), β and $\bar{\rho}$ are given by equation (9b) and s is given by equation (10). This expression is accurate to within 9% for all ρ_o and ω ; it is accurate to within 5% for $\rho_o > 5$.

The optimum condition yielding the minimum of equation (13) is reasonably approximated by

$$\omega_{\min} \approx \frac{8\rho_o^2}{10 + 5\rho_o^{7/3}} \quad (14)$$

for $\rho_o > 1$. The global minimum vanishes for $\rho_o < 1$ (approximately) and is replaced by local minima at the extremes of $\omega = 0$ and $\omega = \rho_o$. The smaller of these minima occurs for $\omega = 0$, so as a practical matter the optimum condition for small radii is usually $\omega = \rho_o$ for $\rho_o < 1$. In this regime, the magnitude of the corresponding minimum is roughly $\delta_o \approx \varepsilon\rho_o$. For larger radii, the magnitude of the minimum displacement first increases, reaches a maximum of $\delta_o/\varepsilon h \approx 1.6$ for $\rho_o \approx 2.3$ and then decays for still larger radii. The condition $\rho_o \approx 2.3$ thus represents the worst-case geometry, but minimum displacements are still large over a very wide range of radii ($\delta_o/\varepsilon h > 1$ for $1 < \rho_o < 8$).

Comparing the results of figures 6 and 8, we see that outer-radius top-surface displacements for annular features are always greater than those for a post or disc, except when the normalized radius ρ_o is about five or more and the normalized feature width ω is less than seven. For $\rho_o < 5$, displacements for annular features are very much larger than for the solid feature when ω is small, and this is due entirely to skewing of the feature walls. Normalized top-surface displacements for annular features at $\omega > 7$ are essentially independent of both the radius and the feature width.

Although these computed displacements on the inner and outer radii of annular features are based on fully axisymmetric geometries, the results should yield good estimates of maximum displacements for arc segments of fixed radius provided that the arc length along the segment is at least several times the resist thickness. This can be expressed as $\bar{\rho}\theta > 5$, where θ is the included angle of the arc. Likewise, they should yield good estimates for displacements along any curved feature provided the change in radius with arc length is small compared to the normalized radius $\bar{\rho}$.

The preceding results all describe displacements of the PMMA, not variation in the dimensions of metal structures. These structure dimensions can be expressed in terms of the PMMA displacements in the form of an overall taper T_m and a mean skew S_m of the centreline of the structure. If the metal were all deposited following complete expansion of the PMMA, this taper and skew would be

$$T_m = \delta_o - \delta_i \quad (15a)$$

and

$$S_m = \frac{\delta_i + \delta_o}{2} \quad (15b)$$

where δ_i and δ_o are the PMMA displacements given above. A positive taper indicates a narrowing at the top of the metal structure; a positive skew indicates radial displacement outward at the top.

5. Comparison with measurements

The only published measurements of PMMA displacements due to absorption and thermal expansion are those of Ruzzu and Matthis [12]. They measured the radial growth at the top of an annular feature subject to submersion in a nickel-sulfamate electrolyte at both 23 and 52 °C. The reported growth of the radius was 3.5 μm for submersion at 23 °C and 7 μm for 52 °C. They did not indicate whether these measurements applied to the inner or outer radius. They also reported radial displacements for a disc, but the disc radius was not specified.

Dimensions of their annulus were $r_i = 1025 \mu\text{m}$, $w = 100 \mu\text{m}$ and $h = 500 \mu\text{m}$. These yield the dimensionless radii $\rho_i = r_i/h = 2.05$ and $\rho_o = r_o/h = (r_i + w)/h = 2.25$; the corresponding dimensionless width is $\omega = w/h = 0.20$ and the parameter beta is $\beta = \omega/\rho_o = 0.089$. For these values, equation (9a) yields $\delta_i/\varepsilon h = 2.4$ for the normalized inner displacement and equation (13) gives $\delta_o/\varepsilon h = 2.6$ for the outer displacement. For submersion at 52 °C in nickel-sulfamate electrolyte, the total linear strain [16] is $\varepsilon \approx 0.0054$ due to water absorption (0.28%) and thermal expansion (0.26%). Based on this value and $h = 500 \mu\text{m}$, the calculated inner and outer displacements are 6.5 and 7.0 μm , respectively, and the mean top-surface radial growth is $(\delta_i + \delta_o)/2 \approx 6.8 \mu\text{m}$. This agrees very well with the measured value of 7 μm reported by Ruzzu and Matthis. For submersion at 23 °C, the total strain is mostly due to water absorption, $\varepsilon \approx 0.0028$ [15]. In this case, the displacements computed using equations (6) and (10) are 3.4 and 3.6 μm for the inner and outer radii, respectively. These yield a mean outward displacement of 3.5 μm , which agrees exactly with the measured value.

Note that the estimated 90% saturation times for this annular feature are about 90 min at 23 °C and only 15 min at 52 °C. These values are based on numerical simulations using measured diffusivities [16] for nickel-sulfamate and take into account exposure to the solution on both the inner and the outer radii. The latter of these results is in good agreement with the observation by Ruzzu and Matthis that the annulus reached maximum diameter in just less than 2 h for submersion at room temperature (their figure 5). Such small times result from the small 100 μm feature width and the fact that both faces of the feature contact the electrolyte. In contrast, the 90% saturation times based on the full 500 μm thickness and electrolyte contact at the top surface only are about 140 h and 27 h at 23 and 52 °C, respectively. Transients resulting in partial saturation during the course of electrodeposition may therefore play an important role in dimensional errors when the resist thickness is large and the lateral extent of PMMA features is large compared to the thickness.

6. Potential remedies

PMMA displacements for any fixed strain can be reduced significantly through the use of auxiliary moat-like channels surrounding mould cavities [13]. Illustrated in figure 9, such channels reduce PMMA displacements and the associated taper of metal structures by reducing the value of w/h for the PMMA features bounding the mould cavity. By equation (1), the thickness of the moat wall (distance w between the cavity

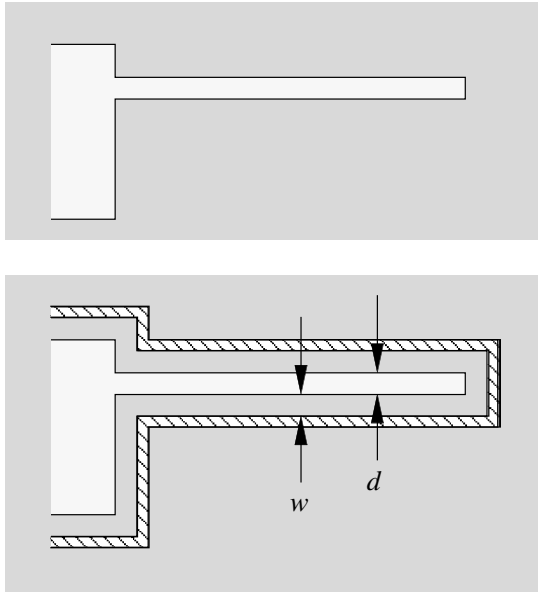


Figure 9. A moat-like relief channel (cross-hatched) patterned into the PMMA surrounding a structure (light) can dramatically reduce sidewall taper if it is placed close to the mould cavity. A moat width at least as large as the PMMA thickness will help ensure that these auxiliary features do not develop slowly due to transport limitations.

and moat) for a linear structure must be small compared to the resist thickness in order for the moat to be highly effective. For an isolated linear structure and no moats, each top-surface displacement is $\delta = 2.3\epsilon h$. For $w/h = 0.5$, the displacement drops to $\delta = 0.33\epsilon h$, and for $w/h = 0.2$ the displacement is just $\delta = 0.13\epsilon h$. In the latter case, the moat reduces displacements by a factor of 18. Such displacements may be acceptably small, but dimensional errors in metal structures nevertheless grow in proportion to the structure height if both the structure width d and normalized moat wall thickness w/h are fixed.

Alternatively, the moat wall thickness can be chosen as a fraction of the width d of the cavity or metal structure. For $w/d = 1$, the relative error in the structure width is $2\delta/d = 1.2\epsilon$ if $h/d > 1$. The relative error in this case is independent of the structure aspect ratio, but the aspect ratio of the moat wall may be large and buckling may occur. Note that the condition $w/d = 1$ is always realized in a uniform grid of lines and spaces having equal widths. As a result, the dimensional accuracy of such grids should always be good provided that buckling does not occur.

The design of moats for curved geometries is more complex. Inner-radius PMMA displacements can be reduced to zero at the top surface by selecting the appropriate value of w/h using equation (12). This will produce a metal structure having an outer radius with zero mean vertical slope, though sidewall deviations along the height of the structure will not vanish. Outer-radius PMMA displacements can be minimized using equation (14), though the minimum displacement will still be large for radii in the range $h < r_o < 8h$.

Moat designs for curved geometries are further complicated by the fact that overall taper and skew of the metal structure trade against one another. Taper is generally

small for small w/h and increases as w/h becomes large. Skew, on the other hand, is large when w/h is small, but is small when w/h is large. Optimum moat designs must therefore consider whether accuracy of structure width or verticality of the structure is more important in a given application. The interested reader can verify these observations using equation (15) and appropriate geometries for the two PMMA features bounding a metal structure.

Moats thus offer a partial solution to the problem of PMMA swelling. They are highly effective in reducing dimensional errors for linear structures and for the outer radius of curved metal structures (inner radius of PMMA); however, they are not very effective in reducing errors on the inner radius of metal structures (outer radius of PMMA). Further, moats cannot be employed in some geometries, as the topology of a metal structure may not allow space for proper moat placement. Moats may also interfere with structure function in some geometries, prohibiting their use altogether. Additional remedies are therefore required.

PMMA swelling is important in optics, and several papers have been published on inorganic coatings to inhibit water absorption [19, 20]. Such coatings will be a challenge for LIGA, however, since they must be applied after development, must be non-conducting, must be conformal in features of high aspect ratio, cannot permanently cover the plating base and must survive prolonged electrolyte exposure. Diffusivities of water in nearly all polymers are within an order of magnitude of that for PMMA, so organic coatings of acceptable thickness are not likely to provide much benefit. This probably includes hydrophobic coatings, as they will directly contact water in the electrolyte regardless of their preference to do otherwise.

Alternatives to linear PMMA as the LIGA x-ray resist may also reduce dimensional errors. Cross-linked PMMA is already established as a viable alternative to linear PMMA for use in LIGA [21, 22], and this may swell less than the linear material due to decreased chain mobility. SU-8 is sometimes employed as an x-ray resist, and water absorption for this should be very low. However, SU-8 has its own issues of dimensional accuracy owing to $\sim 7\%$ shrinkage during post-exposure bake [23]. Polylactides have also been considered for use as an x-ray resist [24]; water absorption for these materials is unknown. Several other polymers are known to absorb very little water, including polyethylene, polystyrene, polysulphone, polyphenyloxide and polytetrafluoroethylene [15]. Most of these will not be suitable as resists because they do not degrade sufficiently in response to radiation, cannot be solvent stripped or because they have a very high coefficient of thermal expansion.

One promising (though untried) remedy for PMMA swelling is to bond the PMMA to the substrate at an elevated temperature. If the PMMA and substrate are bonded at the temperature of electrodeposition, then the thermally-induced displacements during electrodeposition will nominally vanish, even if the x-ray exposure is performed at ambient temperature. The success of this approach will require that the PMMA does not creep between bonding and the completion of electrodeposition. Alternatively, the bonding could be performed at a temperature above that of electrodeposition. In this case, the thermal strain initially present in the PMMA

would offset thermal displacements during electrodeposition and at least a portion of those displacements due to water absorption.

Finally, reducing electrodeposition temperatures from 50 °C to near ambient will reduce dimensional errors by 30 to 40%, but the cost of this is very high. Temperature is one of only two main parameters varied to control electrodeposition processes, and nearly all traditional plating processes are performed at elevated temperature. As such, plating at near-ambient temperature does not seem like a viable long-term remedy to this problem.

7. Summary

Metal structures produced by the LIGA process may exhibit large dimensional errors due to PMMA swelling by thermal expansion and the absorption of water during electrodeposition. These dimensional errors appear mainly in the form of tapered metal structures having a reduced width at the structure top, and the magnitude of this taper may reach $28 \mu\text{m mm}^{-1}$, under the worst conditions, if mitigating measures are not used. PMMA swelling is thus by far the largest single source of dimensional error for the LIGA process.

Top-surface dimensional errors for isolated linear structures bounded by large regions of PMMA are proportional to the product of the strain and structure height. Relative errors in structure width are therefore proportional to the structure aspect ratio, and the magnitude of the error is 14% for an aspect ratio of 10 and a total linear strain of 0.3%. This is the minimum credible strain for water absorption alone and corresponds to electrodeposition at ambient temperature. The maximum credible strain is about 0.6% for electrodeposition at 50 °C, leading to a relative error of 28% at an aspect ratio of 10. In contrast, relative errors in structure width are proportional to the width of the PMMA features bounding the structure when the PMMA widths are small compared to the height. In this case, relative errors grow with increasing strains, but they do not depend on the structure height. Limiting the width of PMMA features defining a metal structure is therefore highly beneficial in reducing dimensional errors.

PMMA swelling also limits the maximum producible aspect ratio of isolated linear metal structures. For a strain of 0.3%, the maximum aspect ratio is about 72; this drops to 36 for a strain of 0.6%. These are the maximum possible aspect ratios because each top-surface sidewall displacement exceeds half the width of the mould cavity for still larger aspect ratios, and the top of the cavity simply closes. Larger aspect ratios may be obtained only if the widths of the PMMA features bounding the cavity are much less than five times the structure height. Swelling additionally limits the maximum aspect ratio of long PMMA features for which buckling does not occur. The maximum aspect ratio of such features is about 20 for a strain of 0.3%; it is only about 14 for a strain of 0.6%.

Dimensional errors for simple holes and posts are again proportional to the product of the strain and thickness when the radius is large compared to the thickness, but are proportional to the strain and the radius when the radius is small. As such, both holes and posts exhibit relative dimensional errors that

are proportional to the structure aspect ratio only when the aspect ratio is small. Relative errors for these geometries are proportional to the total strain, but are independent of both the radius and height when the aspect ratio is large.

Axisymmetric metal structures produced using annular features in a PMMA mould exhibit dimensional errors that depend strongly on whether the sidewall of interest is an inner or outer radius. Top-surface errors on the metal inner radius are always positive and are always large when the radius is larger than the structure height. These errors exhibit a minimum for some optimum width of the PMMA feature that depends only on the radius. In contrast, errors on a metal structure outer radius may be either positive or negative depending on the radius and width of the PMMA feature. These top-surface errors thus vanish for some optimum feature width that depends only on the radius. As a result of this disparity between inner and outer radii, curved metal structures will be tapered, narrowing at the top, but they will also be skewed from the vertical such that the top surface is displaced radially outward.

All of these results are based on an assumption that the PMMA reaches the equilibrium strain early in the electrodeposition period. Thermal diffusivities of PMMA are fairly large, so thermal equilibrium is usually reached within hours. Diffusivities of water in PMMA are very small, however, so equilibrium strains due to water absorption may not be reached for many days when the resist thickness is large and the electrodeposition temperature is low. In these cases, transient swelling may occur throughout the deposition process, and dimensional errors may be reduced significantly.

Acknowledgments

This work was funded by Sandia's Materials Science Research Foundation, the LIGA Technical Maturation Project and the Microsystems Engineering Program. The authors thank Alice Kilgo of Sandia/New Mexico for the image used in figure 1. The structure appearing in this image was produced by the Sandia/Livermore LIGA group using the Advanced Light Source in Berkeley, California. Sandia National Laboratories is operated by Sandia Corporation for the United States Department of Energy under contract DE-AC04-94AL85000.

References

- [1] Becker E W, Ehrfeld W, Hagemann P, Maner A and Munchmeyer D 1986 Fabrication of microstructures with high aspect ratios and great structural heights by synchrotron radiation lithography, galvanofarming and plastic moulding (LIGA process) *J. Microelectron. Eng.* **4** 35–56
- [2] Munchmeyer D and Ehrfeld W 1987 Accuracy limits and potential applications of the LIGA technique in integrated optics *Proc. SPIE* **803** 72–9
- [3] Ehrfeld W, Bley P, Gotz F, Mohr J, Munchmeyer D, Schelb W, Baving H J and Beets D 1988 Progress in deep-etch synchrotron radiation lithography *J. Vac. Sci. Technol. B* **6** 178–82
- [4] Feiertag G, Ehrfeld W, Lehr H, Schmidt A and Schmidt M 1997 Accuracy of structure transfer in deep x-ray lithography *J. Microelectron. Eng.* **35** 557–60

- [5] Feiertag G, Ehrfeld W, Lehr H, Schmidt A and Schmidt M 1998 Calculation and experimental determination of the structure transfer accuracy in deep x-ray lithography *J. Micromech. Microeng.* **7** 323–31
- [6] Pantenburg F J and Mohr J 1995 Influence of secondary effects on the structure quality in deep x-ray lithographie *Nucl. Instrum. Methods B* **97** 551–6
- [7] Pantenburg F J, Achenbach S and Mohr J 1998 Characterization of defects in very high deep-etch x-ray lithography microstructures *Microsyst. Technol.* **4** 89–93
- [8] Griffiths S K and Ting A 2002 The influence of x-ray fluorescence on LIGA sidewall tolerances *Microsyst. Technol.* **8** 120–8
- [9] Zumaque H, Kohring G A and Hormes J 1997 Simulation studies of energy deposition and secondary processes in deep x-ray lithography *J. Micromech. Microeng.* **7** 79–88
- [10] Griffiths S K 2004 Fundamental limitations of LIGA x-ray lithography: sidewall offset, slope and minimum feature size *J. Micromech. Microeng.* **14** 999–1011
- [11] Achenbach S, Pantenburg F J and Mohr J 2003 Numerical simulation of thermal distortions in deep and ultra-deep x-ray lithography *Microsyst. Technol.* **9** 220–4
- [12] Ruzzu A and Matthis B 2002 Swelling of PMMA structures in aqueous solutions and room temperature Ni-electroforming *Microsyst. Technol.* **8** 116–9
- [13] Griffiths S K and Crowell J A W 2003 Dimensional errors in LIGA-produced metal parts due to thermal expansion and swelling of PMMA *Proc. 5th Int. Workshop on High Aspect Ratio Microstructure Technology (HARMST'03)* pp 15–7
- [14] Aigeldinger G, Ceremuga J T and Skala D M 2004 Large batch dimensional metrology demonstrated in the example of a LIGA fabricated spring *Microsyst. Technol.* accepted
- [15] Daniels C A 1989 *Polymers: Structure and Properties* (Lancaster, PA: Technomic Publishing)
- [16] Goods S H, Watson R M and Yi M 2003 Thermal expansion and hydration behavior of PMMA molding materials for LIGA applications *Sandia National Laboratories Report SAND2003–8000*
- [17] *ABAQUS/Standard v6.3*. ABAQUS, Inc. Pawtucket, RI
- [18] Product specification for CQ grade PMMA. Goodfellow Corp. Berwyn, PA
- [19] Jakobs S, Schulz U and Duparre A 1997 Characterization of SiO₂ protective coatings on polycarbonate *Fresenius J. Anal. Chem.* **358** 242–4
- [20] Schulz U and Kaiser N 1997 Near-infrared spectroscopy for monitoring water permeability of optical coatings on plastic *Appl. Opt.* **36** 862–5
- [21] Mohr J, Ehrfeld W and Munchmeyer D 1988 Requirements of resist layers in deep-etch synchrotron radiation lithography *J. Vac. Sci. Technol. B* **6** 2264–7
- [22] Pantenburg F J, Achenbach S and Mohr J 1998 Influence of developer temperature and resist material on the structure quality in deep x-ray lithography *J. Vac. Sci. Technol. B* **16** 3547–51
- [23] Guerin L, Bossel M, Demierre M, Calmes S and Renaud P 1997 Simple and low cost fabrication of embedded microchannels by using a new thick-film photoplastic *Proc. Transducers* 1419–22
- [24] Wollersheim O, Zumaque H, Hormes J, Langen J, Hoessel P, Haussling L and Hoffmann G 1994 Radiation chemistry of poly(lactides) as new polymer resists for the LIGA process *J. Micromech. Microeng.* **4** 84–93